

## Physical, Spectroscopic and Thermal Characterization of Biofield treated Myristic acid

Mahendra Kumar Trivedi<sup>1</sup>, Rama Mohan Tallapragada<sup>1</sup>, Alice Branton<sup>1</sup>, Dahryn Trivedi<sup>1</sup>, Gopal Nayak<sup>1</sup>, Rakesh K. Mishra<sup>2</sup> and Snehasis Jana<sup>2\*</sup>

<sup>1</sup>Trivedi Global Inc., 10624 S Eastern Avenue Suite A-969, Henderson, NV 89052, USA

<sup>2</sup>Trivedi Science Research Laboratory Pvt. Ltd., Hall-A, Chinar Mega Mall, Chinar Fortune City, Hoshangabad Rd., Bhopal- 462026, Madhya Pradesh, India

### Abstract

Myristic acid has been extensively used for fabrication of phase change materials for thermal energy storage applications. The objective of present research was to investigate the influence of biofield treatment on physical and thermal properties of myristic acid. The study was performed in two groups (control and treated). The control group remained as untreated, and biofield treatment was given to treated group. The control and treated myristic acid were characterized by X-ray diffraction (XRD), Differential scanning calorimetry (DSC), Thermogravimetric analysis (TGA), Fourier transform infrared (FT-IR) spectroscopy, and Laser particle size analyzer. XRD results revealed alteration in intensity of peaks as well as significant increase in crystallite size (27.07%) of treated myristic acid with respect to control. DSC study showed increase in melting temperature of treated myristic acid as compared to control. Nevertheless, significant change (10.16%) in latent heat of fusion ( $\Delta H$ ) was observed in treated myristic acid with respect to control. TGA analysis of treated myristic acid showed less weight loss (31.33%) as compared to control sample (60.49%). This may be due to increase in thermal stability of treated myristic acid in comparison with control. FT-IR results showed increase in frequency of  $-CH_2$  and  $C=O$  stretching vibrations, probably associated with enhanced bond strength and force constant of the respective bonds. The particle size analyzer showed significant decrease in average particle size ( $d_{50}$  and  $d_{99}$ ) of treated myristic acid with respect to control. Overall, the results showed significant alteration in physical, spectroscopic and thermal properties of myristic acid. The enhanced crystallite size, and thermal stability of treated myristic acid showed that treated myristic acid could be used as phase change material for thermal energy storage applications.

**Keywords:** Myristic acid; Phase change materials; X-ray diffraction; Thermal stability; Fourier transform infrared spectroscopy; Particle size analysis

**Abbreviation:** XRD: X-ray diffraction; DSC: Differential scanning calorimetry; TGA: Thermogravimetric analysis; DTA: Differential thermal analysis; DTG: Derivative thermogravimetry; FT-IR: Fourier transform infrared; PCMs: Phase change materials

### Introduction

Nowadays, the energy consumption and production has considered as an interesting topic and debatable among researchers. The demand for generation of newer energy sources are increasing steadily day by day. This calls for design and development of novel energy saving devices in order to reduce the consumption of energy [1]. The enormous increase in production of greenhouse gases in atmosphere and elevation in cost of fossil fuel have caused researchers to develop more efficient thermal energy storage devices. Thermal energy storage has grabbed significant attention worldwide for energy conservation from the available sources of heat [2,3]. Phase change materials (PCM) are known as substance with high latent heat of fusion, which are capable of storing and releasing large amount of energy whenever required. Phase change materials (PCMs) are smart devices that can be utilized for thermal energy storage. Moreover, form stable phase change PCMs are especially interesting due to high latent heat, shape stable and it can be directly used without encapsulation methods [4]. The materials used for fabricating the form stable solid-liquid PCMs are organic compounds such as paraffin [5], fatty acids [6], fatty alcohol [7,8], polyethylene glycol and their mixtures [9,10].

Fatty acids are commonly obtained from natural resources such as vegetable and animal oil products. These compounds have wide applicability in cosmetics, washing, environmental clean-up,

encapsulation and drug delivery [11]. Additionally, fatty acids possess excellent properties such as high phase change enthalpy and tunable phase change nature [12]. Myristic acid has recently showed great potential as solid-liquid PCMs for thermal energy storage applications [13,14]. Hence, by considering the phase change property of myristic acid, authors decided to investigate the influence of biofield treatment on its physical, spectroscopic and thermal properties which can be further utilized for thermal storage applications.

Fritz, has first proposed the law of mass-energy interconversion and after that Einstein derived the well-known equation  $E=mc^2$  for light and mass [15,16]. Though, conversion of mass into energy is fully validated, but the inverse of this relation, *i.e.* energy into mass is not yet verified scientifically. Additionally, it was stated that energy exist in various forms such as kinetic, potential, electrical, magnetic, nuclear etc. which have been generated from different sources. Similarly, neurons which are present in human brain have the ability to transmit the information in the form of electrical signals [17-20]. Thus, human beings have the ability to harness the energy from environment/Universe and can transmit into any object (living or non-living) around the Globe. The

**\*Corresponding author:** Jana S, Trivedi Science Research Laboratory Pvt. Ltd., Hall-A, Chinar Mega Mall, Chinar Fortune City, Hoshangabad Rd., Bhopal- 462026, Madhya Pradesh, India, Tel: +91-755-6660006; E-mail: [publication@trivedisrl.com](mailto:publication@trivedisrl.com)

Received August 03, 2015; Accepted August 20, 2015; Published August 27, 2015

**Citation:** Trivedi MK, Tallapragada RM, Branton A, Trivedi D, Nayak G et al. (2015) Physical, Spectroscopic and Thermal Characterization of Biofield treated Myristic acid. J Fundam Renewable Energy Appl 5: 180. doi:10.4172/20904541.1000180

**Copyright:** © 2015 Trivedi MK, et al. This is an open-access article distributed under the terms of the Creative Commons Attribution License, which permits unrestricted use, distribution, and reproduction in any medium, provided the original author and source are credited.

object(s) always receive the energy and respond into a useful manner that is called biofield energy. This whole process is known as biofield treatment. Mr. Trivedi is known to transform the characteristics of various living and nonliving things. The biofield treatment has altered the physical and thermal properties in metals [21-24], improved the growth and production of agriculture crops [25-28] and significantly altered the phenotypic characteristics of various pathogenic microbes [29-31]. Additionally, biofield treatment has substantially altered the medicinal, growth and anatomical properties of ashwagandha [32].

By conceiving above mentioned excellent outcome from biofield treatment and phase change property of myristic acid, this work was undertaken to investigate the impact of biofield on physical, spectroscopic and thermal properties of myristic acid.

## Materials and Methods

Myristic acid was procured from Sisco Research Laboratories (SRL), India. The sample was divided into two parts; one was kept as a control sample, while the other was subjected to Mr. Trivedi's biofield treatment and coded as treated sample (T). The treatment group (T) was in sealed pack and handed over to Mr. Trivedi for biofield treatment under laboratory condition. Mr. Trivedi provided the treatment through his energy transmission process to the treated group without touching the sample. The control and treated samples were characterized by XRD, DSC, TGA, FT-IR, and particle size analysis.

## Characterization

### X-ray diffraction (XRD) study

XRD analysis of control and treated myristic acid was carried out on Phillips, Holland PW 1710 X-ray diffractometer system, which had a copper anode with nickel filter. The radiation of wavelength used by the XRD system was 1.54056 Å. The data obtained from this XRD were in the form of a chart of  $2\theta$  vs. intensity and a detailed table containing peak intensity counts,  $d$  value (Å), peak width ( $\theta^\circ$ ), relative intensity (%) etc. The crystallite size ( $G$ ) was calculated by using formula:

$$G = k\lambda / (b \cos \theta)$$

Here,  $\lambda$  is the wavelength of radiation used,  $b$  is full width half maximum (FWHM) of peaks and  $k$  is the equipment constant (=0.94). Percentage change in crystallite size was calculated using following formula:

$$\text{Percentage change in crystallite size} = [(G_t - G_c) / G_c] \times 100$$

Where,  $G_c$  and  $G_t$  are crystallite size of control and treated powder samples respectively.

### Differential scanning calorimetry (DSC) study

DSC was used to investigate the melting temperature and latent heat of fusion ( $\Delta H$ ) of samples. The control and treated myristic acid samples were analyzed by using a Pyris-6 Perkin Elmer DSC on a heating rate of 10°C/min under air atmosphere and air was flushed at a flow rate of 5 mL/min.

Percentage change in latent heat of fusion was calculated using following equations:

$$\% \text{ change in Latent heat of fusion} = \frac{[\Delta H_{\text{Treated}} - \Delta H_{\text{Control}}]}{\Delta H_{\text{Control}}} \times 100$$

Where,  $\Delta H_{\text{Control}}$  and  $\Delta H_{\text{Treated}}$  are the latent heat of fusion of control and treated samples, respectively.

## Thermogravimetric analysis-differential thermal analysis (TGA-DTA)

Thermal stability of control and treated Myristic acid were analyzed by using Mettler Toledo simultaneous TGA and Differential thermal analyzer (DTA). The samples were heated from room temperature to 400°C with a heating rate of 5°C/min under air atmosphere.

## FT-IR spectroscopy

FT-IR spectra were recorded on Shimadzu's Fourier transform infrared spectrometer (Japan) with frequency range of 4000-500  $\text{cm}^{-1}$ . The treated sample was divided in two parts T1 and T2 for FT-IR analysis.

## Particle size analysis

The average particle size and particle size distribution were analyzed by using Sympetac Helos-BF laser particle size analyzer with a detection range of 0.1 micrometer to 875  $\mu\text{m}$ . Average particle size  $d_{50}$  and  $d_{99}$  (size exhibited by 99% of powder particles) were computed from laser diffraction data table. The  $d_{50}$  and  $d_{99}$  values were calculated by the following formula:

$$\text{Percentage change in } d_{50} \text{ size} = 100 \times (d_{50} \text{ treated} - d_{50} \text{ control}) / d_{50} \text{ control}$$

$$\text{Percentage Change in } d_{99} \text{ size} = 100 \times (d_{99} \text{ treated} - d_{99} \text{ control}) / d_{99} \text{ control}$$

## Results and Discussion

### XRD study

XRD diffractogram of myristic acid (control and treated) are shown in Figure 1. XRD diffractogram of control sample showed intense crystalline peaks at  $2\theta$  equals to 18.58°, 18.93°, 20.18°, 20.79°, 21.51°, 23.92°, and 37.80°. However, the treated myristic acid showed alteration in intensity of the XRD peaks. The XRD data of the myristic acid was well supported by the literature [13]. The XRD peaks of treated sample were observed at  $2\theta$  equals to 18.62°, 18.93°, 20.74°, 21.51°, 23.80°, 23.97° and 37.65°. The result showed that control and treated myristic acid both has  $\gamma$  pattern  $\alpha$  pattern after crystallization [33]. The crystallite size was calculated using Scherrer formula (crystallite size =  $k\lambda / b \cos \theta$ ) and the result are presented in Figure 2. The crystallite size of control myristic acid was 61.58 nm and it was increased to 78.26 nm in treated sample. The result showed that crystallite size was increased significantly by 27.07% in treated myristic acid as compared to control. It was reported previously that increase in processing temperature significantly affects the crystallite size of the materials. The increase in temperature causes decrease in dislocation density and increase in number of unit cell which ultimately causes increase in crystallite size [34,35]. It is hypothesized that biofield may provide some thermal energy that possibly cause elevation in crystallite size of treated myristic acid with respect to control.

Additionally, recently it was showed that introduction of ultrasound to materials leads to substantial increase in crystallite size [36]. Hence, it is assumed that biofield treatment may provide electromagnetic waves similar like ultrasound to treated myristic acid atoms that led to increase in crystallite size with respect to control.

## Thermal analysis

### DSC study

DSC was conducted to investigate the melting nature and latent

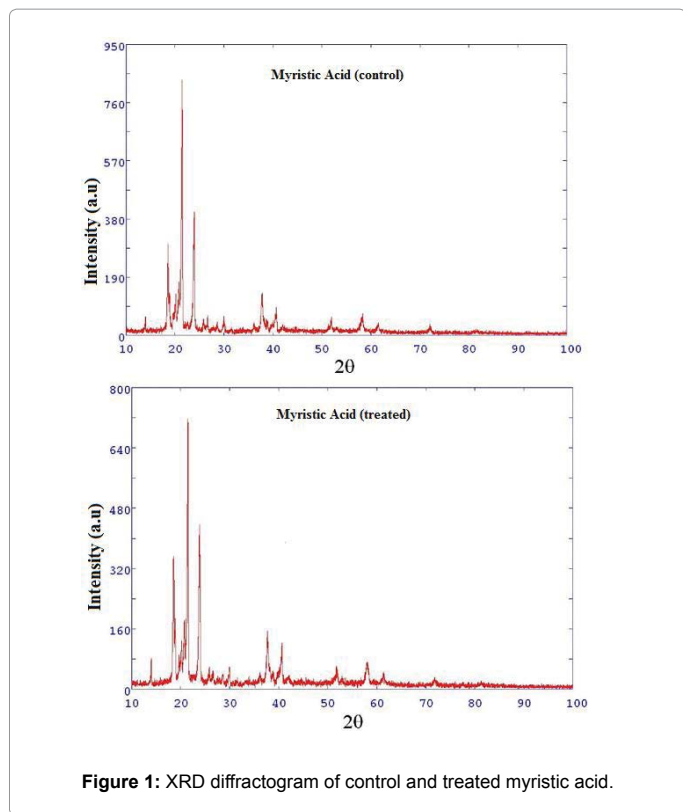


Figure 1: XRD diffractogram of control and treated myristic acid.

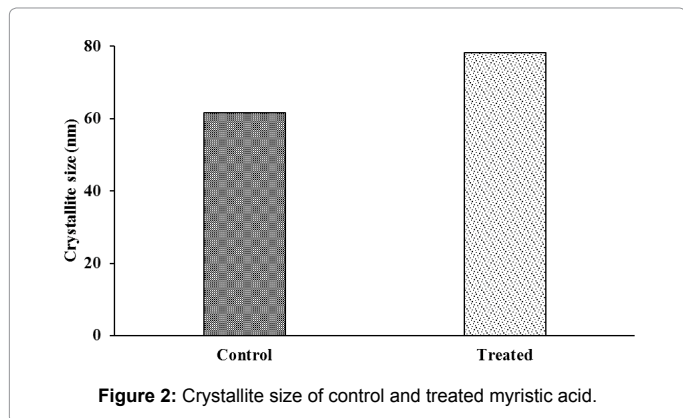


Figure 2: Crystallite size of control and treated myristic acid.

heat of fusion of control and treated myristic acid. DSC thermogram of control myristic acid shows (Figure 3) an intense endothermic inflexion at 55.95°C; attributed to melting temperature of myristic acid. The melting temperature of myristic acid was well supported by the literature [37]. However, the treated myristic acid showed a melting endothermic peak at 57.10°C. It is assumed that increase in melting temperature may be due to interaction of treated myristic acid with biofield energy. It was previously reported that melting temperature of a material depends on its kinetic energy. Hence, it is assumed here that biofield may cause alteration in kinetic energy of treated myristic acid that led to increase in melting temperature. The latent heat of fusion ( $\Delta H$ ) was calculated from the DSC thermograms and results are presented in Table 1. The control myristic acid showed a  $\Delta H$  of 211.43 J/g; however after biofield treatment it was changed to 190.15 J/g. The latent heat of fusion was decreased by 10.16% in treated sample as compared to control. Sari and Kaygusuz showed that myristic acid

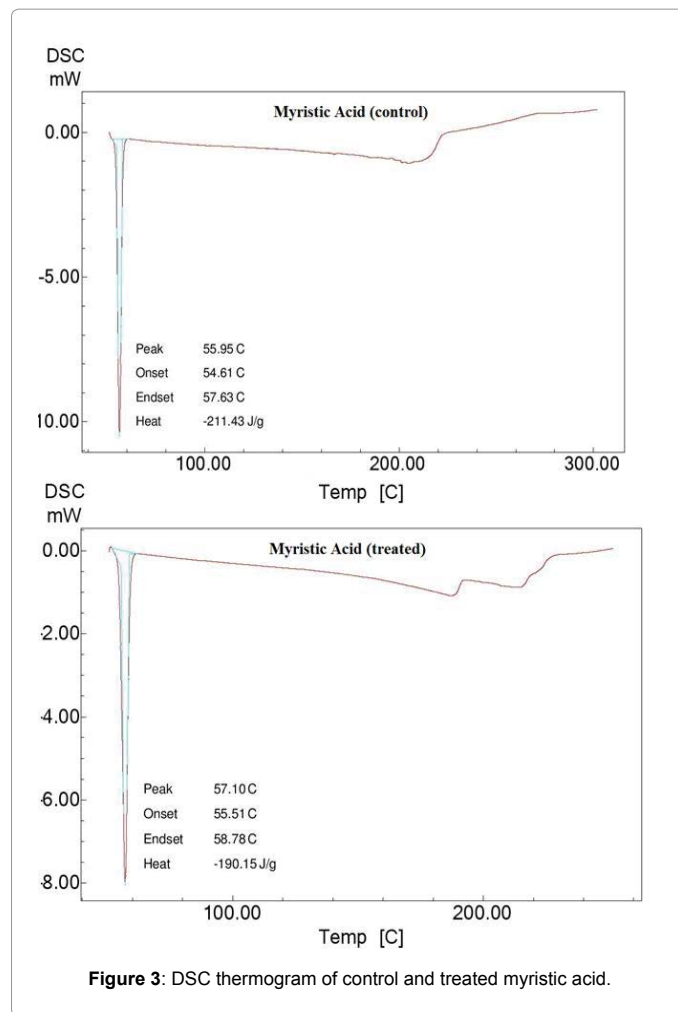


Figure 3: DSC thermogram of control and treated myristic acid.

has a suitable melting point of 49-51°C and a high latent heat of fusion [38]. They stated that myristic acid is good for thermal energy storage for domestic solar water systems [38]. Hence, in the present work the biofield treated myristic acid showed increase in melting temperature and appreciable latent heat of fusion which may be utilized for PCMs for thermal energy storage applications.

### TGA Study

TGA was used to get further insights about the thermal stability of the control and treated myristic acid. TGA thermogram of control and treated myristic acid are shown in Figure 4. The thermogram of control myristic acid showed single step thermal degradation pattern. The onset temperature was noticed at around 196°C and the thermal degradation was stopped at around 237°C. During this step the control myristic acid lost 60.49% of its weight. However, the treated myristic acid also showed one step thermal degradation pattern. The sample started to degrade at around 182°C and the degradation terminated at around 237°C. The thermogram showed 31.33% of weight loss during this step. This showed that % weight loss of myristic acid was decreased after biofield treatment and this may be inferred as improvement in thermal stability of treated sample. Sharma et al., mentioned that good thermal stability, cheap and wide availability of fatty acids allows them to be used as PCMs [39]. Hence, it is presumed here that biofield treated myristic acid could be a good prospect as PCMs.

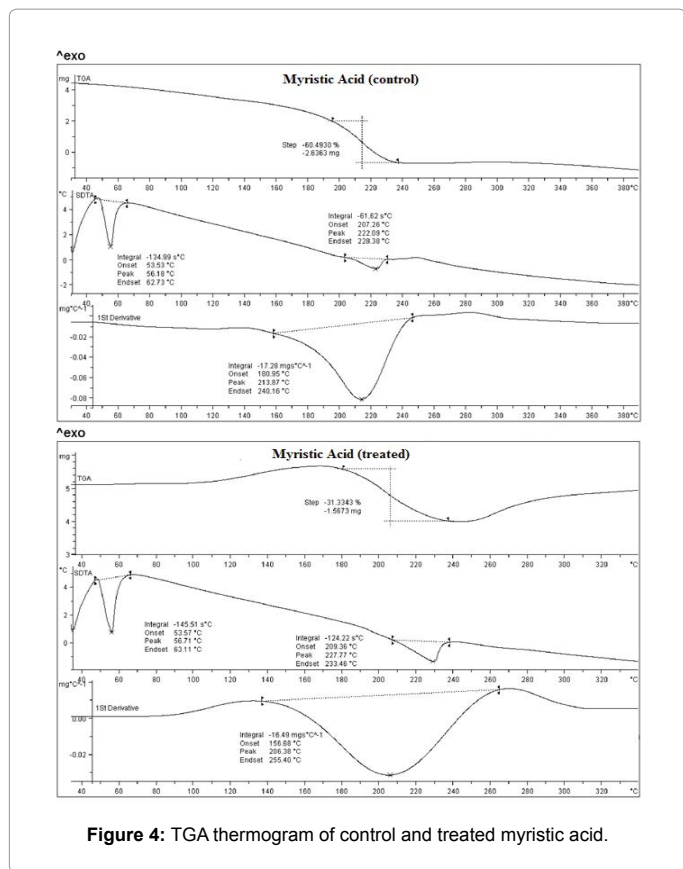


Figure 4: TGA thermogram of control and treated myristic acid.

The DTA thermogram of control myristic acid showed two endothermic peaks at 56.18°C and 222.09°C. The former peak attributed to melting of the myristic acid and second peak represented the thermal decomposition of the compound. However, the DTA thermogram of treated myristic acid showed two endothermic peaks; first one corresponded to melting endotherm (56.71°C) and second peak was due to thermal decomposition (227.77°C). Derivative thermogravimetry (DTG) of control myristic acid showed maximum thermal decomposition temperature ( $T_{max}$ ) at 213.87°C; however it was decreased in treated myristic acid (206.38°C) (Table 1). Hence, the DTG result of treated myristic acid showed no improvement in  $T_{max}$  after biofield treatment.

### FT-IR spectroscopy

FT-IR spectrum of control and treated myristic acid are presented in Figures 5 and 6, respectively. The control myristic acid showed band corresponding to C=O stretching vibration at 1701  $cm^{-1}$ . Other peaks at 2916 and 2848 were due to symmetrical and asymmetrical stretching of  $-CH_2$  functional group in fatty acid. The stretching peaks at 686, 721 and 939  $cm^{-1}$  were due to  $-OH$  swinging or rocking mode, which were characteristics of aliphatic chain of myristic acid [40]. The FT-IR peaks at 1431, and 1464  $cm^{-1}$  were due to  $-CH_2$  bending vibration peaks. Other peaks were observed at 1286 and 1261  $cm^{-1}$  represents the C-H and C-C bending vibrations, respectively.

FT-IR spectrum of treated myristic acid T1 and T2 are presented in Figure 6. FT-IR spectrum of T1 showed typical absorption peaks of  $-CH_2$  stretching vibrations at 2916 and 2848  $cm^{-1}$ . Likewise, to control the peak at 1701, 1431 and 1464  $cm^{-1}$  were due to C=O group stretching and  $-CH_2$  bending vibrations. The absorption peaks at 1286 and 1261

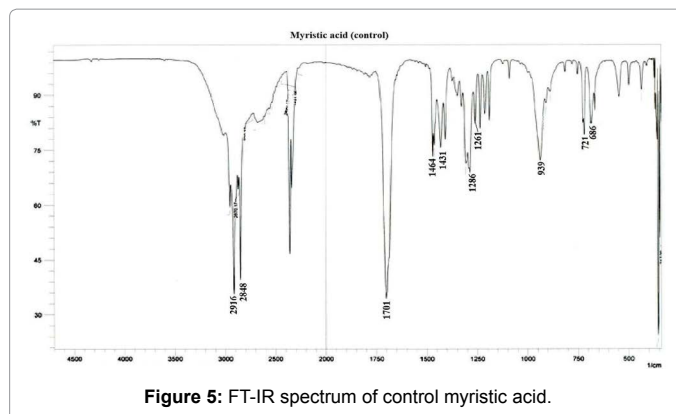


Figure 5: FT-IR spectrum of control myristic acid.

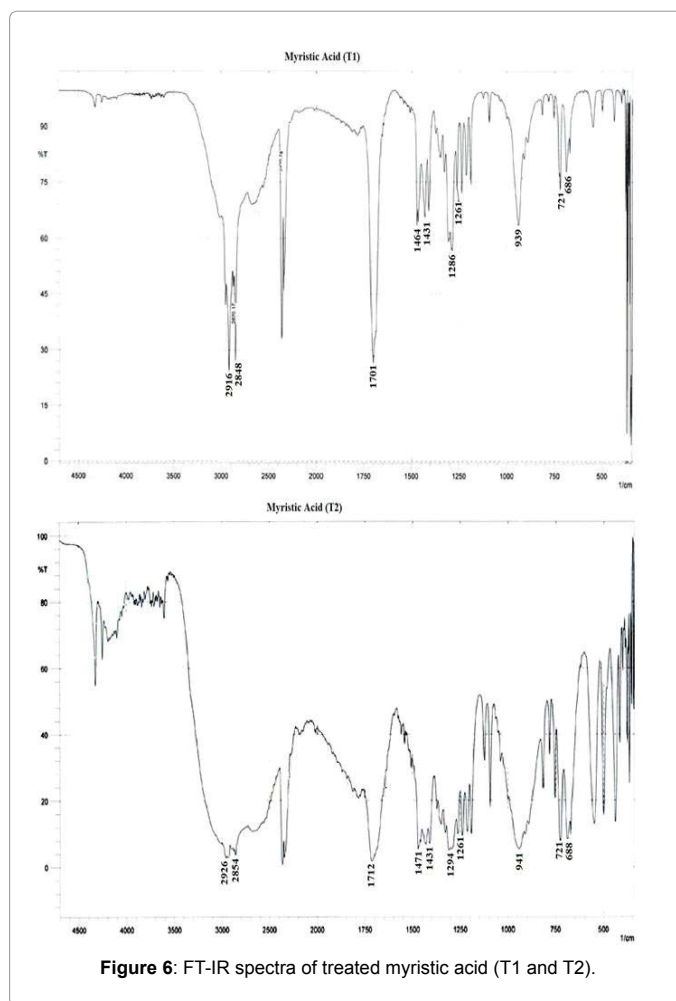


Figure 6: FT-IR spectra of treated myristic acid (T1 and T2).

$cm^{-1}$  corresponded to C-H and C-C bending vibrations, respectively. The FT-IR peaks at 686, 721, and 939  $cm^{-1}$  were due to  $-OH$  swinging or rocking vibrations. This showed no significant difference in FT-IR peaks of control and T1 myristic acid sample.

Whereas, the T2 sample showed substantial upward shifting of the FT-IR peaks of 2916→2926  $cm^{-1}$  ( $-CH_2$  stretch), 2848→2854  $cm^{-1}$  ( $-CH_2$  stretch), and 1701→1712 (C=O stretch). It was previously suggested that the frequency ( $\nu$ ) of vibrational peak depends on two factors i.e. force constant and reduced mass [41]. If mass is constant then frequency is

directly proportional to force constant, hence, increase in frequency of any bond may cause possible enhancement in force constant of respective bond and *vice versa*. Hence, it is assumed that increase in frequency of  $-CH_2$  and  $C=O$  groups in T2 sample may increase the force constant and strength of these bonds. Moreover, the FT-IR of T2 also showed upward shifting of  $-CH_2$  bending ( $1464 \rightarrow 1471 \text{ cm}^{-1}$ ) and  $C-C$  bending ( $1286 \rightarrow 1294 \text{ cm}^{-1}$ ) which may be due to some changes in chemical nature of the sample. Overall, the FT-IR results of treated myristic acid (T2) showed substantial alteration in bond strength and force constant after biofield treatment which may improve the stability of treated sample with respect to control.

### Particle size analysis

Particle size of myristic acid (control and treated) was calculated from particle size distribution graph and presented in Figures 7 and 8. The average particle size ( $d_{50}$ ) of control myristic acid was  $63.19 \mu\text{m}$  and it was decreased to  $21.67 \mu\text{m}$  in treated sample (Figure 7). Additionally, the  $d_{99}$  value (size exhibited by 99% of the particles) was decreased significantly in treated myristic acid  $135.25 \mu\text{m}$  as compared to control myristic acid ( $679.95 \mu\text{m}$ ). The  $d_{50}$  and  $d_{99}$  both were altered significantly by 65.7% and 80.1%, respectively in treated myristic acid

(Figure 8). The biofield treatment may cause fracture in the bigger size microparticles which led to reduction in particle size of treated myristic acid as compared to control.

### Conclusion

The result showed significant impact of biofield treatment on physical, spectroscopic and thermal properties of myristic acid. XRD showed substantial increase in crystallite size of treated myristic acid with respect to control. DSC study on treated myristic acid showed increase in melting temperature with respect to control. A significant change in latent heat of fusion (10.16%) was observed in treated myristic acid as compared to control. TGA analysis revealed the lowering in weight loss of treated myristic acid as compared to control, which corroborated its high thermal stability. FT-IR spectroscopic study showed the alteration in force constant and bond strength of treated myristic acid with respect to control. Moreover, the biofield treated myristic acid showed decrease in particle size that may enhance the surface area as compared to control sample. Therefore, high melting temperature, thermal stability and appreciable latent heat of fusion of treated myristic acid may improve the phase change nature and it could be used for fabrication of thermal energy storage devices. Although, future studies such as thermal conductivity measurement can be further design to study the potential of biofield treated myristic acid for these applications.

### Acknowledgement

The authors like to acknowledge the Trivedi Science, Trivedi Master Wellness and Trivedi Testimonials for their steady support during the work. This should be included in acknowledgment.

### References

- Feng L, Zheng J, Yang H, Guo Y, Li W, et al. (2011) Preparation and characterization of polyethyleneglycol/active carbon composites as shape-stabilized phase change materials. *Sol Energ Mat Sol C* 95: 644-650.
- Chen C, Liu K, Wang H, Liu W, Zhang H (2013) Morphology and performances of electrospun polyethyleneglycol/poly (dl-lactide) phase change ultrafine fibers for thermal energy storage. *Sol Energ Mat Sol C* 117: 372-381.
- Wang C, Feng L, Li W, Zheng J, Tian W, et al. (2012) Shape-stabilized phase change materials based on polyethyleneglycol /porous carbon composite: the influence of the pore structure of the carbon materials. *Sol Energ Mat Sol C* 105: 21-26.
- Kenisarin MM, Kenisarina KM (2012) Form-stable phase change materials for thermal energy storage. *Renew Sust Energ Rev* 16: 1999-2040.
- Zhang P, Hu Y, Song L, Ni J, Xing W, et al. (2010) Effect of expanded graphite on properties of high-density polyethylene/paraffin composite with in tumescent flame retardant as shape-stabilized phase change material. *Sol Energ Mat Sol C* 94: 360-365.
- Fang G, Li H, Chen Z, Liu X (2011) Preparation and properties of palmitic acid/SiO<sub>2</sub> composites with flame retardant as thermal energy storage materials. *Sol Energ Mat Sol C* 95: 1875-1881.
- Zeng JL, Zhang J, Liu YY, Cao ZX, Zhang ZH, et al. (2008) Polyaniline/1- tetra decanol composites. *J Therm Anal Calorim* 91: 455-461.
- Zeng JL, Liu YY, Cao ZX, Zhang J, Zhang ZH, et al. (2008) Thermal conductivity enhancement of MWNTs on the PANI/tetradecanol form-stable PCM. *J Therm Anal Calorim* 91: 443-446.
- Karaman S, Karaipekli A, Sari A, Biçer A (2011) Polyethylene glycol (PEG)/ diatomite composite as a novel form-stable phase change material for thermal energy storage. *Sol Energ Mat Sol C* 95: 1647-1653.
- Karaipekli A, Sari A (2008) Capric-myristic acid/expanded perlite composite as form-stable phase change material for latent heat thermal energy storage. *Renew Energ* 33: 2599-2605.
- Fameau AL, Arnould A, Saint-Jalmes A (2014) Responsive self-assemblies

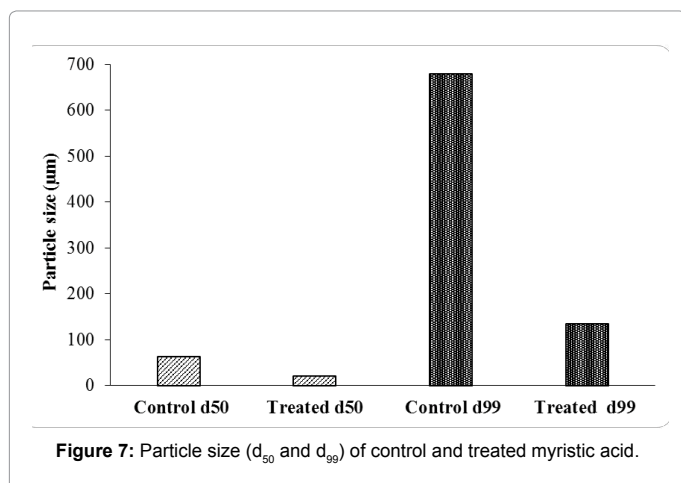


Figure 7: Particle size ( $d_{50}$  and  $d_{99}$ ) of control and treated myristic acid.

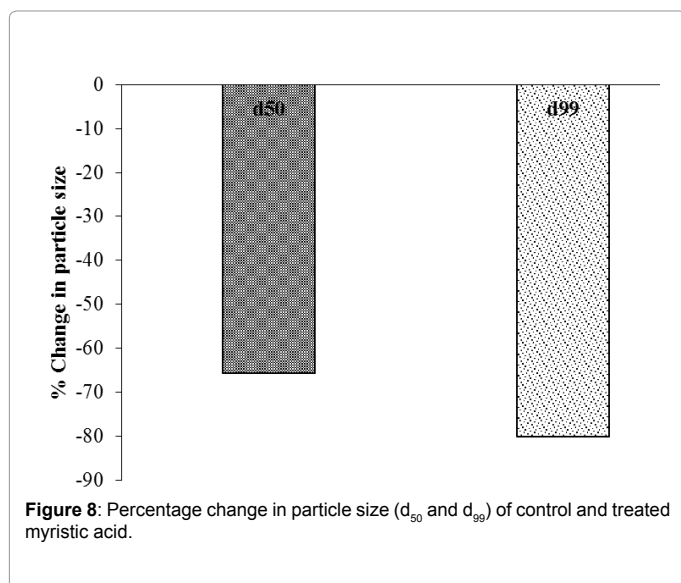


Figure 8: Percentage change in particle size ( $d_{50}$  and  $d_{99}$ ) of control and treated myristic acid.

- based on fatty acids. *Curr Opin Colloid Interface Sci* 19: 471-479.
12. Yuan Y, Zhang N, Tao W, Cao X, He Y (2014) Fatty acids as phase change materials: A review. *Renew Sust Energy Rev* 29: 482-498.
  13. Zeng J, Zhu F, Yu S, Xiao Z, Yan W, et al. (2013) Myristic acid/polyaniline composites as form stable phase change materials for thermal energy storage. *Sol Energy Mat Sol C* 114: 136-140.
  14. Chen C, Liu X, Liu W, Ma M (2014) A comparative study of myristic acid/bentonite and myristic acid/Eudragit L100 form stable phase change materials for thermal energy storage. *Sol Energy Mat Sol C* 127: 14-20.
  15. Hasenohrl F (1904) On the theory of radiation in moving bodies. *Ann Phys (Berlin)* 15: 344-370.
  16. Einstein A (1905) Does the inertia of a body depend upon its energy-content? *Ann Phys (Berlin)* 18: 639-641.
  17. Becker RO, Selden G (1985) *The body electric: electromagnetism and the foundation of life*, William Morrow and Company, New York City.
  18. Barnes RB (1963) Thermography of the human body. *Science* 140: 870-877.
  19. Born M (1971) *The Born-Einstein Letters*. (1stedn), Walker and Company, New York.
  20. Cohen S, Popp FA (2003) Biophoton emission of the human body. *Indian J Exp Biol* 41: 440-445.
  21. Trivedi MK, Patil S, Tallapragada RM (2013) Effect of biofield treatment on the physical and thermal characteristics of vanadium pentoxide powders. *J Material Sci Eng S11*: 001.
  22. Trivedi MK, Patil S, Tallapragada RM (2013) Effect of biofield treatment on the physical and thermal characteristics of silicon, tin and lead powders. *J Material Sci Eng* 2: 125.
  23. Trivedi MK, Patil S, Tallapragada RM (2014) Atomic, crystalline and powder characteristics of treated zirconia and silica powders. *J Material Sci Eng* 3: 144.
  24. Trivedi MK, Patil S, Tallapragada RMR (2015) Effect of biofield treatment on the physical and thermal characteristics of aluminium powders. *Ind Eng Manag* 4: 151.
  25. Shinde V, Sances F, Patil S, Spence A (2012) Impact of biofield treatment on growth and yield of lettuce and tomato. *Aust J Basic Appl Sci* 6: 100-105.
  26. Sances F, Flora E, Patil S, Spence A, Shinde V (2013) Impact of biofield treatment on ginseng and organic blueberry yield. *Agrivita J Agric Sci* 35: 22-29.
  27. Lenssen AW (2013) Biofield and fungicide seed treatment influences on soybean productivity, seed quality and weed community. *Agricultural Journal* 8: 138-143.
  28. Patil SA, Nayak GB, Barve SS, Tembe RP, Khan RR (2012) Impact of biofield treatment on growth and anatomical characteristics of *Pogostemon cablin* (Benth.). *Biotechnology* 11: 154-162.
  29. Trivedi MK, Patil S (2008) Impact of an external energy on *Staphylococcus epidermis* [ATCC –13518] in relation to antibiotic susceptibility and biochemical reactions – An experimental study. *J Accord Integr Med* 4: 230-235.
  30. Trivedi MK, Patil S (2008) Impact of an external energy on *Yersinia enterocolitica* [ATCC –23715] in relation to antibiotic susceptibility and biochemical reactions: An experimental study. *Internet J Alternative Med* 6: 2.
  31. Trivedi MK, Bhardwaj Y, Patil S, Shettigar H, Bulbule A (2009) Impact of an external energy on *Enterococcus faecalis* [ATCC – 51299] in relation to antibiotic susceptibility and biochemical reactions – An experimental study. *J Accord Integr Med* 5: 119-130.
  32. Nayak G, Altekar N(2015) Effect of biofield treatment on plant growth and adaptation. *J Environ Health Sci* 1: 1-9.
  33. Hua D, Zhang X, Zhan G, Hong Y, Su Y, et al. (2014) A high-pressure polar light microscopy to study the melt crystallization of myristic acid and ibuprofen in CO<sub>2</sub>. *J Supercrit Fluids* 87: 22-27.
  34. Gaber A, Abdel-Rahim MA, Abdel-Latif AY, Abdel-Salam MN (2014) Influence of calcination temperature on the structure and porosity of nanocrystalline SnO<sub>2</sub> synthesized by a conventional precipitation method. *Int J Electrochem Sci* 9: 81-95.
  35. Raj KJA, Viswanathan B (2009) Effect of surface area, pore volume, particle size of P25 titania on the phase transformation of anatase to rutile. *Indian J Chem* 48A: 1378-1382.
  36. Cherepanov PV, Melnyk I, Andreeva DV (2015) Effect of high intensity ultrasound on Al<sub>3</sub>Ni<sub>2</sub>, Al<sub>3</sub>Ni crystallite size in binary AlNi (50 wt% of Ni) alloy. *Ultrason Sonochem* 23: 26-30.
  37. Ince S, Seki Y, Ezan MA, Turgut A, Ereğ A (2015) Thermal properties of myristic acid/graphite nanoplates composite phase change materials. *Renew Energy* 75: 243-248.
  38. Sari A, Kaygusuz K (2001) Thermal performance of myristic acid as a phase change material for energy storage application. *Renew Energy* 24: 303-317.
  39. Sharma A, Tyagi VV, Chen CR, Buddhi D (2009) Review on thermal energy storage with phase change materials and applications. *Renew Sust Energy Rev* 13: 318-345.
  40. Yang X, Yuan Y, Zhang N, Cao X, Liu C (2014) Preparation and properties of myristic–palmitic–stearic acid/expanded graphite composites as phase change materials for energy storage. *Sol Energy* 99: 259-266.
  41. Pavia DL, Lampman GM, Kriz GS (2001) *Introduction to spectroscopy*. (3rd edn), Thomson learning, Singapore.